Gate-modulated thermoelectric conversion in disordered nanowires: I. Low temperature coherent regime

Riccardo Bosisio, Geneviève Fleury, Jean-Louis Pichard

Gate-modulated thermoelectric conversion in disordered nanowires: I. Low temperature coherent regime

Riccardo Bosisio, Geneviève Fleury, and Jean-Louis Pichard
Service de Physique de l'État Condensé (CNRS URA 2464), IRAMIS/SPEC, CEA Saclay, 91191 Gif-sur-Yvette, France

We study the thermopower of a disordered nanowire in the presence of an external gate electrode which can be used for depleting the carrier density inside the nanowire. In this first paper, we study the low temperature regime where the electron transport remains elastic through a disordered nanowire described by a one-dimensional tight-binding Anderson model. The gate voltage is depicted by a uniform on-site potential which can be varied for shifting the impurity band of the nanowire. The thermopower is evaluated using a Sommerfeld expansion valid below a characteristic temperature which depends on the gate potential. In the limit where the length of the nanowire exceeds the localization length, the typical thermopower is given by three analytical expressions describing the cases where the electron transport takes place (i) inside the impurity band of the nanowire, (ii) around its band edges and eventually (iii) outside its band. Notably we highlight that the typical thermopower is strongly enhanced at the band edges, an analytical formula obtained by Derrida and Gardner for describing the energy dependence of the localization length around the band edges allowing us to perfectly describe the edge behavior of the thermopower. Then, we investigate the mesoscopic fluctuations of the thermopower around its typical value. Inside the impurity band, they are given by a Lorentzian distribution, with a width proportional to the density of states evaluated at the Fermi energy. As the band edges are approached, we find a transition towards a Gaussian distribution. Eventually, the implications of our results for the low temperature figure of merit and the output power of disordered nanowires are discussed.

PACS numbers: 72.20.Pa 73.63.Nm 73.23.-b

I. INTRODUCTION

Semiconductor nanowires have emerged for a few years as promising thermoelectric devices[1]. In comparison to their bulk counterparts, they provide opportunities to enhance the dimensionless figure of merit $ZT = S^2\sigma T/\kappa$, which governs the efficiency of thermoelectric conversion at a given temperature T. Indeed, they allow to reduce the phonon contribution κ_{ph} to thermal conductivity κ[2–4]. On the other hand, they offer through their highly peaked density of states the large electron-hole asymmetry required for the enhancement of the thermopower S[5,6]. This makes them now rank, with other nanostructured materials, among the best thermoelectrics in terms of achievable values of ZT. Yet, maximizing the figure of merit is not the ultimate requirement on the quest for improved thermoelectrics. The actual electric power that can be extracted from a heat engine (or conversely the actual cooling power that can be obtained from a Peltier refrigerator) is also of importance when thinking of practical applications. From that point of view, nanowire-based thermoelectric devices are also promising: They offer the scalability needed for increasing the output power, insofar as they can be arranged in arrays of nanowires in parallel.

The main issue of the present paper and the subsequent one[7] is the determination of the dopant density optimizing the thermoelectric conversion in a single semiconductor nanowire. From the theory side, this question has been mainly discussed at room temperature when the semi-classical Boltzmann theory can be used[8–10] or in the ballistic regime[11] when the presence of the disorder is completely neglected. The goal was to describe the thermoelectric properties of nanowires at room temperature where the quantum effects become negligible, and in particular to probe the role of their geometry (diameter, aspect ratio, orientation, ...). From the experimental side, investigations have been carried out by varying the carrier density in the nanowire with an external gate electrode[6,12–15]. Recently, Brovman *et al* have measured at room temperature the thermopower of Silicon and Silicon-Germanium nanowires and observed a strong increase when the nanowires become almost depleted under the application of a gate voltage[16]. Interestingly, this work points out the importance of understanding thermoelectric transport near the band edges of semiconductor nanowires. It also reveals a lack of theoretical framework to this field that we aim at filling.

In that purpose, we shall first identify as a function of the temperature T and the applied gate voltage V_g the dominant mechanism of electronic transport through a given nanowire. At low temperature $T < T_x$, transport is dominated by elastic tunneling processes and quantum effects must be properly handled. Due to the intrinsic disorder characterizing doped semiconductors, the electronic transport is much affected by Anderson localization while the phonon contribution to the thermoelectric coefficients can be neglected. Above the activation temperature T_x, inelastic effects inside the nanowire start to be relevant. One enters the Variable Range Hopping (VRH) regime[17] where phonons help electrons to jump from one localized state to another, far away in space but quite close in energy. At temperatures higher than the

Mott temperature T_M, the VRH regime ceases and one has simple thermal-activation between nearest neighbor localized states. The different regimes are sketched in Fig. 1 for a nanowire modeled by a one-dimensional (1D) tight-binding Anderson model. Note that they are highly dependent on the gate voltage V_g. The VRH regime will be addressed in a following paper[7].

In this work, we focus our study to the elastic regime or more precisely, to a subregion $T < T_s$ inside the elastic regime in which the thermopower can be evaluated using the Landauer-Büttiker scattering formalism and Sommerfeld expansions. We will mainly consider nanowires of size N longer than their localization length ξ. Such a limit is characterized by exponentially small values of the electrical conductance. Obviously, this drastically reduces the output power associated with the thermoelectric conversion. To avoid this exponential reduction, one should take shorter lengths ($N \approx \xi$). Nevertheless, considering $N \gg \xi$, one takes a limit where the nanowire typical transmission at an energy E is simply given by $\exp[-2N/\xi(E)]$. Moreover, in the limit of weak disorder, expansions can be made and the energy function $\xi(E)$ is analytically known both inside the impurity band of the nanowire and around its band edges. This makes possible to derive analytical expressions describing the typical behavior of the thermopower when $N \gg \xi$. To study thermoelectric conversion in the crossover regime $N \approx \xi$ where the transmission does not behave exactly as $\exp[-2N/\xi(E)]$ would require to use the scaling theory discussed in Ref.[18,19]. Moreover, another reason to consider $N \gg \xi$ is that the delay time distribution (which probes how the scattering matrix depends on energy) has been shown to have a universal form[20] in this limit. We expect that this should be also the case for the fluctuations of the thermopower (which probes how the transmission depends on energy). This gives the theoretical reasons for focusing our study to the limit $N \gg \xi$, despite the interest of the crossover regime $N \approx \xi$ for optimizing the thermoelectric conversion.

The outline of the manuscript is as follows. Section II is a reminder about the Landauer-Büttiker formalism which allows to calculate thermoelectric coefficients in the coherent regime. In section III, we introduce the model and outline the numerical method used in this work, which is based on a standard recursive Green's function algorithm. Our results are presented in sections IV, V, VI and VII. Section IV is devoted to the study of the typical behavior of the thermopower as the carrier density in the nanowire is modified with the gate voltage. We show that the thermopower is drastically enhanced when the nanowire is being depleted and we provide an analytical description of this behavior in the localized limit. In section V, we extend the study to the distribution of the thermopower. We show that the thermopower is always Lorentzian distributed, as long as the nanowire is not completely depleted by the applied gate voltage and provided it is long enough with respect to the localization length. Interestingly, the mesoscopic

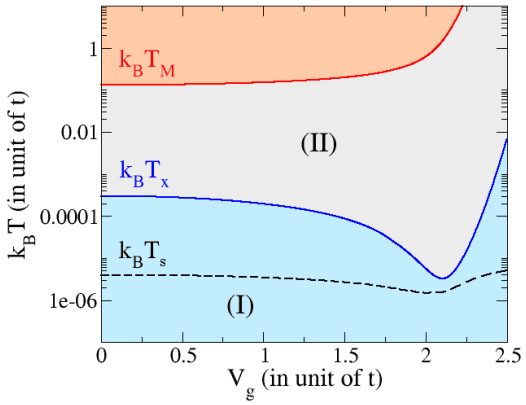

FIG. 1: (Color online) Typical temperature scales separating the different regimes of electronic transport (elastic regime ($T < T_x$, blue), VRH regime ($T_x < T < T_M$, gray) and activated regime ($T > T_M$, red)) through a disordered nanowire. V_g is the external gate voltage which allows to lower the carrier density in the nanowire (it is completely depleted at $V_g = 2.5t$). This paper is restricted to the study of region (I) at $T < T_s$ where the Sommerfeld expansion can be applied for the calculation of the thermoelectric coefficients. Region (II) of VRH will be studied in Ref.[7]. The temperature scales T_s, $T_x = \xi/(2\nu N^2)$ and $T_M = 1/(\xi\nu)$ are plotted for the 1D model introduced in Sec. III with $E_F = 0$, $W = t$ and $N = 1000$. T_s is given for $\epsilon = 0.01\%$ (see Sec. VII).

fluctuations appear to be basically larger and larger as the carrier density in the nanowire is lowered and the typical thermopower increases. As a matter of course, this ceases to be true when the gate voltage is so large that the nanowire, emptied of carriers, behaves eventually as a (disordered) tunnel barrier. In that case, the thermopower distribution is found to be Gaussian with tiny fluctuations. In section VI, we discuss the potential of our results for thermoelectric applications by analyzing the figure of merit ZT and the maximal output power Q of the device. The evaluation of the "crossover temperature" T_s (see Fig. 1) is the subject of section VII. Finally, we draw our conclusions in section VIII.

II. THERMOELECTRIC TRANSPORT COEFFICIENTS IN THE LANDAUER-BÜTTIKER FORMALISM

We consider a conductor connected via reflectionless leads to two reservoirs L (left) and R (right) in equilibrium at temperatures T_L and T_R, and chemical potentials μ_L and μ_R. To describe the thermoelectric transport across the conductor, we use the Landauer-Büttiker formalism[21]. The heat and charge transport are supposed to be mediated only by electrons and the phase coherence of electrons during their propagation through the conductor is supposed to be preserved. In this approach, the dissipation of energy takes place exclusively in the reservoirs while the electronic transport across the

conductor remains fully elastic. The method is valid as long as the phase-breaking length (mainly associated to electron-electron and electron-phonon interactions) exceeds the sample size. From a theoretical point of view, it can be applied to (effective) non-interacting models. In this framework, the electric (I_e) and heat (I_Q) currents flowing through the system are given by[22]

$$I_e = \frac{e}{h}\int dE\,\mathcal{T}(E)[f_L(E) - f_R(E)] \tag{1}$$

$$I_Q = \frac{1}{h}\int dE\,(E-\mu_L)\mathcal{T}(E)[f_L(E) - f_R(E)] \tag{2}$$

where $f_\alpha(E) = (1+\exp[(E-\mu_\alpha)/(k_B T_\alpha)])^{-1}$ is the Fermi distribution of the lead α and $\mathcal{T}(E)$ is the transmission probability for an electron to tunnel from the left to the right terminal. k_B is the Boltzmann constant, $e<0$ the electron charge and h the Planck constant. The above expressions are given for spinless electrons and shall be doubled in case of spin degeneracy.

We now assume that the differences $\Delta\mu = \mu_L - \mu_R$ and $\Delta T = T_L - T_R$ to the equilibrium values $E_F \approx \mu_L \approx \mu_R$ and $T \approx T_L \approx T_R$ are small. Expanding the currents in Eqs. (1, 2) to first order in $\Delta\mu$ and ΔT around E_F and T, one obtains[22]

$$\begin{pmatrix} I_e \\ I_Q \end{pmatrix} = \begin{pmatrix} L_0 & L_1 \\ L_1 & L_2 \end{pmatrix} \begin{pmatrix} \Delta\mu/eT \\ \Delta T/T^2 \end{pmatrix} \tag{3}$$

where the linear response coefficients L_i are given by

$$L_i = \frac{e^2}{h} T \int dE\,\mathcal{T}(E) \left(\frac{E-E_F}{e}\right)^i \left(-\frac{\partial f}{\partial E}\right). \tag{4}$$

The electrical conductance G, the (electronic contribution to the) thermal conductance κ_e, the Seebeck coefficient $\mathcal{S}$ (or thermopower) and the Peltier coefficient Π can all be expressed in terms of the Onsager coefficients L_i as

$$G \equiv \left.\frac{eI_e}{\Delta\mu}\right|_{\Delta T=0} = \frac{L_0}{T} \tag{5}$$

$$\kappa_e \equiv \left.\frac{I_Q}{\Delta T}\right|_{I_e=0} = \frac{L_0 L_2 - L_1^2}{T^2 L_0} \tag{6}$$

$$\mathcal{S} \equiv -\left.\frac{\Delta\mu}{e\Delta T}\right|_{I_e=0} = \frac{L_1}{T L_0} \tag{7}$$

$$\Pi \equiv \left.\frac{I_Q}{I_e}\right|_{\Delta T=0} = \frac{L_1}{L_0}\ . \tag{8}$$

The Seebeck and Peltier coefficients turn out to be related by the Kelvin-Onsager relation[23,24]

$$\Pi = \mathcal{S}T \tag{9}$$

as a consequence of the symmetry of the Onsager matrix. Note that, by virtue of Eq. (4), in presence of particle-hole symmetry we have $\mathcal{S} = \Pi = 0$. Further, the link between the electrical and thermal conductances is quantified by the Lorenz number $\mathcal{L} = \kappa_e/GT$.

In the zero temperature limit $T \to 0$, the Sommerfeld expansion[25] can be used to estimate the integrals (4). To the lowest order in $k_B T/E_F$, the electrical conductance reduces to $G \approx \frac{e^2}{h}\mathcal{T}(E_F)$ while the thermopower simplifies to

$$\mathcal{S} \approx \frac{\pi^2}{3}\frac{k_B}{e}\,k_B T\,\left.\frac{\mathrm{d}\ln\mathcal{T}}{\mathrm{d}E}\right|_{E_F}. \tag{10}$$

The Lorenz number $\mathcal{L}$ takes in this limit a constant value,

$$\mathcal{L} \approx \mathcal{L}_0 \equiv \frac{\pi^2}{3}\left(\frac{k_B}{e}\right)^2, \tag{11}$$

as long as $|\mathcal{S}| \ll \sqrt{\mathcal{L}_0} \simeq 156\,\mu\mathrm{V.K}^{-1}$. This reflects the fact that the electrical and thermal conductances are proportional and hence cannot be manipulated independently, an important although constraining property known as the Wiedemann-Franz (WF) law. This law is known to be valid for non-interacting systems if the low temperature Sommerfeld expansion is valid[26,27], when Fermi liquid (FL) theory holds[25,28] and for metals at room temperatures[25], while it could be largely violated in interacting systems due to non FL behaviors[29,30].

III. MODEL AND METHOD

The system under consideration is sketched in Fig. 2(a). It is made of a 1D disordered nanowire coupled via perfect leads to two reservoirs L (left) and R (right) of non-interacting electrons, in equilibrium at temperature $T_L = T + \Delta T$ [$T_R = T$] and chemical potential $\mu_L = E_F + \Delta\mu$ [$\mu_R = E_F$]. The nanowire is modeled as a 1D Anderson chain of N sites, with lattice spacing $a = 1$. Its Hamiltonian reads,

$$\mathcal{H} = -t\sum_{i=1}^{N-1}\left(c_i^\dagger c_{i+1} + \mathrm{h.c.}\right) + \sum_{i=1}^{N}\epsilon_i c_i^\dagger c_i\,, \tag{12}$$

where $c_i^\dagger$ and c_i are the creation and annihilation operators of one electron on site i and t is the hopping energy. The disorder potentials ϵ_i are (uncorrelated) random numbers uniformly distributed in the interval $[-W/2, W/2]$. The two sites at the ends of the nanowire are connected with hopping term t to the leads which can be 1D semi-infinite chains or 2D semi-infinite square lattices, with zero on-site potentials and the same hopping term t. The simpler case of the Wide Band Limit (WBL) approximation, where the energy dependence of the self-energies of the leads is neglected, is also considered. Finally, an extra term

$$\mathcal{H}_{gate} = \sum_i V_g c_i^\dagger c_i \tag{13}$$

is added in the Hamiltonian (12) to mimic the presence of an external metallic gate. It allows to shift the whole impurity band of the nanowire.

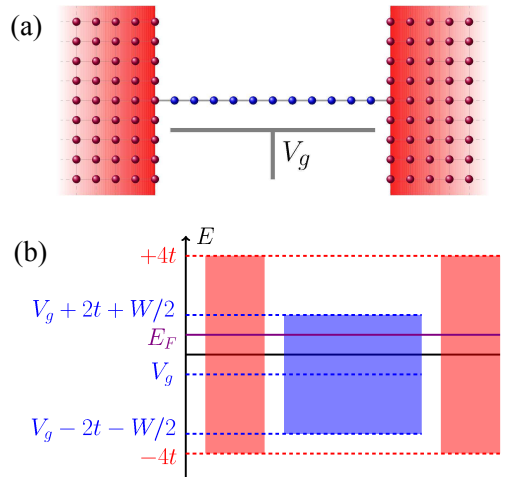

FIG. 2: (Color online) (a) Sketch of the system: a 1D nanowire made of N sites is connected to two leads at its extremities. An external gate voltage V_g is applied. (b) Band diagram. The impurity band of the nanowire (in blue) can be shifted by the application of V_g in order to probe either the bulk, the edges or the outside of the impurity band at Fermi energy E_F. Here, the leads are bidimensional (conduction band of the leads in red) and hence, $E_F \in [-4t, 4t]$.

A. Recursive Green's function calculation of the transport coefficients

In the Green's function formalism, the transmission $\mathcal{T}(E)$ of the system at an energy E is given by the Fisher-Lee formula[21]

$$\mathcal{T}(E) = \mathrm{Tr}[\Gamma_L(E) G(E) \Gamma_R(E) G^\dagger(E)] \qquad (14)$$

in terms of the retarded single particle Green's function $G(E) = [E - \mathcal{H} - \Sigma_L - \Sigma_R]^{-1}$ and of the retarded self-energies Σ_L and Σ_R of the left and right leads. The operators $\Gamma_\alpha = i(\Sigma_\alpha - \Sigma_\alpha^\dagger)$ describe the coupling between the conductor and the lead $\alpha = L$ or R. A standard recursive Green's function algorithm[31] allows us to compute the transmission $\mathcal{T}(E)$. The logarithmic derivative $\mathrm{d}\ln\mathcal{T}/\mathrm{d}E$ can be calculated as well with the recursive procedure, without need for a discrete evaluation of the derivative. It yields the thermopower $\mathcal{S}$ in the Mott-Sommerfeld approximation (10). Let us precise, to settle the notations, that in the following we will refer to a dimensionless thermopower

$$S = -t \left.\frac{\mathrm{d}\ln\mathcal{T}}{\mathrm{d}E}\right|_{E_F} \qquad (15)$$

which is related, in the Mott-Sommerfeld approximation, to the thermopower $\mathcal{S}$ in physical units as

$$\mathcal{S} = \frac{\pi^2}{3}\left(\frac{k_B}{|e|}\right)\left(\frac{k_B T}{t}\right) S\,. \qquad (16)$$

We now discuss the expressions of the self-energies $\Sigma_L(E)$ and $\Sigma_R(E)$ of the left and right leads which are to be given as input parameters in the recursive Green's function algorithm. The nanowire of length N sites is supposed to be connected on one site at its extremities to two identical leads, which are taken 1D, 2D or in the WBL approximation. Hence, the self-energies Σ_α (as well as the operator Γ_α) are $N \times N$ matrices with only one non-zero component (identical for both leads) that we denote with Σ (or Γ). When the wide-band limit is assumed for the leads, Σ is taken equal to a small constant imaginary number independent of the energy E. When the leads are two 1D semi-infinite chains or two 2D semi-infinite square lattices, Σ is given by the retarded Green's function G_{lead} of the lead under consideration evaluated at the site X (in the lead) coupled to the nanowire, $\Sigma = t^2 \langle X | G_{\mathrm{lead}} | X \rangle$. Knowing the expressions of the retarded Green's functions of the infinite 1D chain and the infinite 2D square lattice[32], it is easy to deduce G_{lead} for the semi-infinite counterparts by using the method of mirror images. For 1D leads, one finds $\Sigma(E) = -te^{ik(E)}$ where $E = -2t\cos k$ and k is the electron wavevector[21]. For 2D leads, the expression of $\Sigma(E)$ is more complicated (see Appendix A). As far as the Fermi energy E_F is not taken near the edges of the conduction band of the leads, the thermopower behaviors using 1D and 2D leads coincide with those obtained using the WBL approximation (see Sec. IV). This shows us that the dimensionality D becomes irrelevant in that limit, and we expect that taking 3D leads will not change the results.

B. Scanning the impurity band of the Anderson model

The density of states per site $\nu(E)$ of the Anderson model, obtained by numerical diagonalization of the Hamiltonian (12), is plotted in Fig. 3(a) in the limit of large N. It is non-zero in the interval $[E_c^-, E_c^+]$ where $E_c^\pm = \pm(2t + W/2)$ are the edges of the impurity band. In the bulk of the impurity band (*i.e.* for energies $|E| \lesssim 1.5t$), the density of states is given with a good precision by the formula derived for a clean 1D chain (red dashed line in Fig. 3(a)),

$$\nu_b(E) = \frac{1}{2\pi t\sqrt{1 - (E/2t)^2}}\,. \qquad (17)$$

As one approaches the edges $E_c^\pm$, the disorder effect cannot be neglected anymore. The density of states is then well described by the analytical formula obtained by Derrida and Gardner around $E_c^\pm$, in the limit of weak disorder and large N (see Ref.[33]),

$$\nu_e(E) = \sqrt{\frac{2}{\pi}}\left(\frac{12}{tW^2}\right)^{1/3} \frac{\mathcal{I}_1(X)}{[\mathcal{I}_{-1}(X)]^2} \qquad (18)$$

where $X = (|E| - 2t)t^{1/3}(12/W^2)^{2/3}$ and

$$\mathcal{I}_n(X) = \int_0^\infty y^{n/2}\, e^{-\frac{1}{6}y^3 + 2Xy}\, dy\,. \qquad (19)$$

In Fig. 3(a), the small discrepancy between the numerical data (circles) and the analytical formula (18) (blue line) is attributed to the relatively large value of disorder $W = t$ considered in the figure; it fades out for smaller disorder values. In a tiny energy interval only, very close to the band edges $E_c^{\pm}$, may be identified Lifshitz tails. They correspond to the exponential cancellation of the density of states in the close neighborhood of $E_c^{\pm}$. They are not highlighted in Fig. 3(a).

In this paper, we study the behavior of the thermoelectric coefficients as one probes at the Fermi energy E_F electron transport either inside or outside the impurity band, and more particularly in the vicinity of the band edges. Such a scan of the impurity band can be done in two ways. One possibility is to vary the position of the Fermi energy E_F in the leads. Doing so, we modify the distance between E_F and the band edges $E_c^{\pm}$ but also the one between E_F and the band edges of the leads. This can complicate the analysis of the data, the dimensionality of the leads becoming relevant when $|E_c^{\pm} - E_F| \to 0$. To avoid this complication, we can keep E_F fixed far from $E_c^{\pm}$ and vary the gate voltage V_g (see Fig. 2(b)).

C. Localization length of the Anderson model

In the disordered 1D model (12) we consider, all eigenstates are exponentially localized, with a localization length ξ. As a consequence, the typical transmission of the nanowire drops off exponentially with its length N. More precisely, when $N \gg \xi$ (localized limit), the distribution of $\ln \mathcal{T}$ is a Gaussian[34,35] centered around the value

$$[\ln \mathcal{T}]_0(E) = -\frac{2N}{\xi(E)}\,, \tag{20}$$

as long as the energy E of the incoming electron is inside the impurity band of the nanowire. The inverse localization length $1/\xi$ can be analytically obtained as a series of integer powers of W when $W \to 0$. To the leading order (see e.g.[36]), this gives

$$\xi_b(E) = \frac{24}{W^2}\left(4t^2 - E^2\right)\,. \tag{21}$$

The formula is known to be valid in the weak disorder limit inside the bulk of the impurity band (hence the index b). Strictly speaking, it fails in the vicinity of the band center $E = 0$ where the perturbation theory does not converge[37] but it gives nevertheless a good approximation. As one approaches one edge of the impurity band, the coefficients characterizing the expansion of $1/\xi$ in integer powers of W diverge and the series has to be reordered. As shown by Derrida and Gardner[33], this gives (to leading order in W) the non analytical behavior $1/\xi \propto W^{2/3}$ as one edge is approached instead the analytical behavior $1/\xi \propto W^2$ valid in the bulk of the impurity band. More precisely, one find in the limit

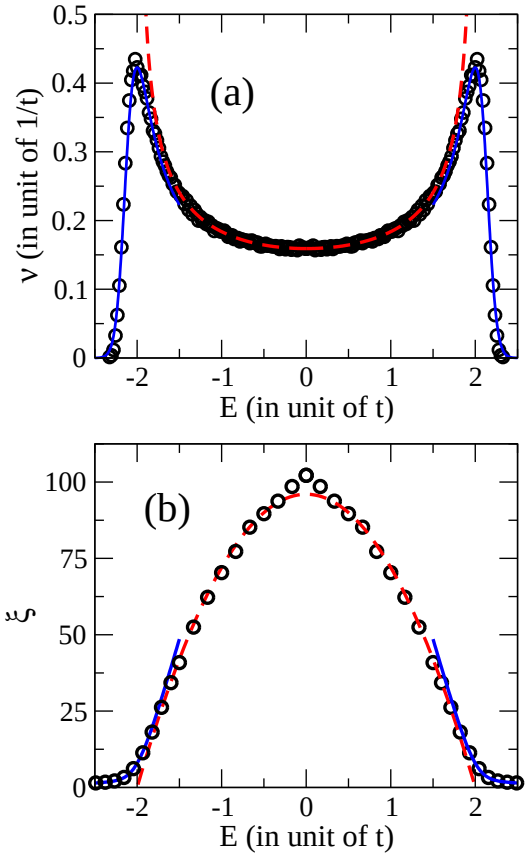

FIG. 3: (a) Density of states per site ν as a function of energy E for the 1D Anderson model (12) with disorder amplitude $W/t = 1$, in the limit $N \to \infty$. The circles correspond to numerical data (obtained with $N = 1600$). The red dashed line and the blue line are the theoretical predictions (17) and (18), expected in the bulk and at the edges of the manowire conduction band. (b) Localization length ξ of the 1D Anderson model (12) (with $W/t = 1$) as a function of energy E. The circles correspond to numerical data (obtained with Eq. (20)). The red dashed line and the blue line are the theoretical predictions (21) and (22).

$W \to 0$ that

$$\xi_e(E) = 2\left(\frac{12t^2}{W^2}\right)^{1/3}\frac{\mathcal{I}_{-1}(X)}{\mathcal{I}_1(X)} \tag{22}$$

as E approaches the band edges $\pm 2t$. $\mathcal{I}_i$ are integrals defined in Eq. (19) and X a parameter introduced just above this equation. As shown in Fig. 3(b), both formula (21) and (22) are found to be in very good agreement with our numerical evaluation of $\xi(E)$, in the respective range of energy that they describe, even outside a strictly weak disorder limit ($W = t$ in Fig. 3(b)).

IV. TYPICAL THERMOPOWER

We compute numerically the thermopower S for many realizations of the disorder potentials ϵ_i in Eq. (12), and

we define the *typical* value S_0 as the median of the resulting distribution $P(S)$. As it will be shown in Sec. V, $P(S)$ is typically a smooth symmetric function (Lorentzian or Gaussian), and thus its median coincides with its most probable value. We study the behavior of S_0 as one scans the energy spectrum of the nanowire by varying the position of the Fermi energy E_F in the leads or the gate voltage V_g.

In Fig. 4(a), the typical thermopower S_0 of a long nanowire in the localized regime is plotted as a function of E_F and at $V_g = 0$. Since $S_0 \to -S_0$ when $E_F \to -E_F$, data are shown for positive values of E_F only. In the figure, three different kinds of leads are considered: 1D leads, 2D leads or leads in the WBL approximation. In all cases, as expected, we find that $S_0 = 0$ at the center of the conduction band of the leads ($E_F = 0$). Indeed, the random potentials being symmetrically distributed around a zero value, one has a statistical particle-hole symmetry at the band center and the thermopower can only be a statistical fluctuation around a zero typical value. As E_F is increased, the statistical particle-hole symmetry breaks down and S_0 gets finite. Here $S_0 > 0$ because charge transport is dominated by holes for $E_F > 0$. When the wide band limit is assumed for both leads (triangles in Fig. 4(a)), we find that the typical thermopower S_0 increases with E_F and reaches a maximum just before the edge $E_c^+ = 2t + W/2$ ($E_c^+ = 2.5\,t$ in Fig. 4(a) where $W = t$) before decreasing. The same curve is obtained with 1D [2D] leads as long as the Fermi energy E_F remains far enough below the upper band edge of the D-dimensional leads. When E_F approaches $2t$ [$4t$], the typical thermopower S_0 of the nanowire is found to increase drastically, contrary to the WBL case (of course, no data are available for $|E_F| \geq 2t\,[4t]$, charge transfer being impossible outside the conduction band of the leads). This singularity at the band edge of the leads can be easily understood using Eqs. (14) and (15) and noticing that for 1D [2D] leads, $\mathrm{d}\ln\Gamma/\mathrm{d}E \to -\infty$ as $E \to 2t$ [$4t$]. This is obvious in the case of 1D leads where $\Gamma(E) = 2t\sqrt{1-(E/2t)^2}$ and it can also be shown for 2D leads. We will see in Sec. VII that this apparent divergence of the thermopower is actually only valid in an infinitesimally small range of temperatures above 0 K.

With the gate voltage V_g, we can explore the impurity band of the nanowire while keeping E_F fixed. The behavior of S_0 as a function of V_g is shown in Fig. 4(b) for $E_F = 0$ and 1D leads. It is found to be identical to the behavior of S_0 as a function of E_F obtained at $V_g = 0$ in the WBL approximation. This remains true if 2D leads are used in Fig. 4(b) and we have no doubt that it also remains true with 3D leads. Moreover, the results are unchanged if E_F is fixed to any other value, as long as it does not approach too closely one edge of the conduction band of the leads (but it can be chosen close enough to one band edge to recover the continuum limit of the leads). Our main observation is that the typical thermopower S_0 increases importantly when the Fermi energy probes the region around the edges of the impurity band of the nanowire. Qualitatively, this is due to the fact that the typical transmission of the nanowire drops down when the edges are approached: this huge decrease results in a enhancement of the typical thermopower, the thermopower being somehow a measure of the energy dependence of the transmission. A quantitative description of this behavior can also be obtained. Indeed, since the distribution of the transmission $\mathcal{T}$ is log-normal in the localized regime[34,35] and the thermopower S is calculated for each disorder configuration with the Mott approxi-

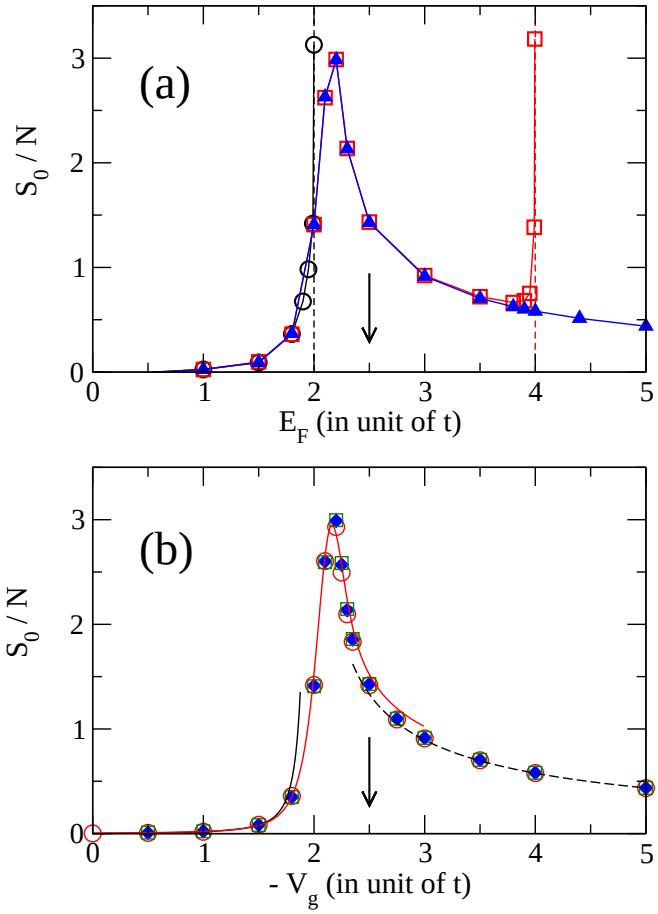

FIG. 4: (Color online) Typical value of the dimensionless thermopower per unit length, S_0/N, as a function of the Fermi energy E_F at $V_g = 0$ (a) and as a function of the gate voltage V_g at $E_F = 0$ (b). In panel (a), the data were obtained at fixed $N = 500$, by using either 1D leads (○), 2D leads (□) or the wide-band limit approximation (▲). With 1D [2D] leads, the typical thermopower shows a divergent behavior at the band edge of the leads (black [red] vertical dashed line). In panel (b), 1D leads are used. The symbols stand for different lengths of the nanowire ($N = 200$ (○), 800 (□) and 1600 (♦)). The full black line, the full red line and the dashed black line correspond respectively to the theoretical fits (24), (25) and (27) expected when E_F probes the bulk, the edge and the outside of the impurity band. In both panels, $W/t = 1$. The arrows indicate the position of the edge of the impurity band of the nanowire.

mation (15), one expects to have

$$S_0 = -t\,\frac{\mathrm{d}[\ln \mathcal{T}]_0}{\mathrm{d}E}\bigg|_{E_F} \tag{23}$$

where $[\ln \mathcal{T}]_0$ is the median of the $\ln \mathcal{T}$ Gaussian distribution (which in this case coincides with the most probable value). Moreover, according to Eq. (20), the energy dependence of $[\ln \mathcal{T}]_0$ is given by the energy dependence of the localization length, *i.e.* by Eqs. (21) and (22). This allows us to derive the following expressions for the typical thermopower in the bulk and at the edges:

$$S_0^b = N\frac{(E_F - V_g)\,W^2}{96t^3[1-((E_F-V_g)/2t)^2]^2}, \tag{24}$$

$$S_0^e = 2N\left(\frac{12t^2}{W^2}\right)^{1/3}\left\{\frac{\mathcal{I}_3(X)}{\mathcal{I}_{-1}(X)} - \left[\frac{\mathcal{I}_1(X)}{\mathcal{I}_{-1}(X)}\right]^2\right\}, \tag{25}$$

where now X is modified to

$$X = (|E_F - V_g| - 2t)t^{1/3}(12/W^2)^{2/3} \tag{26}$$

in order to take into account the effect of the gate voltage V_g. When the outside of the impurity band, rather than the inside, is probed at E_F (i.e. when the wire is completely depleted), no more states are available in the nanowire to tunnel through. Electrons coming from one lead have to tunnel directly to the other lead through the disordered barrier of length N. We have also calculated the typical thermopower of the nanowire in that case, assuming that the disorder effect is negligible (see Appendix B). We find

$$\frac{S_0^{TB}}{N} \underset{N\to\infty}{\approx} -\frac{1}{N}\frac{2t}{\Gamma(E_F)}\,\frac{\mathrm{d}\Gamma}{\mathrm{d}E}\bigg|_{E_F} \mp \frac{1}{\sqrt{\left(\frac{E_F-V_g}{2t}\right)^2 - 1}} \tag{27}$$

with a + sign when $E_F \le V_g - 2t$ and a − sign when $E_F \ge V_g + 2t$. Fig. 4(b) shows a very good agreement between the numerical results (symbols) and the expected behaviors (Eqs. (24), (25) and (27)). One consequence of these analytical predictions is that the peak in the thermopower curves gets higher and narrower as the disorder amplitude is decreased (and vice-versa). We note incidentally that our findings look in qualitative agreement with the recent experimental observation reported in Ref[16]. We stress out however that those measurements were carried out outside the low temperature coherent regime which consider, at room temperatures. To describe them, inelastic effects must be included. It will be the purpose of our next paper[7].

V. THERMOPOWER DISTRIBUTIONS

In the coherent elastic regime we consider, the sample-to-sample fluctuations of the thermopower around its typical value are expected to be large. The most striking illustration occurs at $E_F = V_g$, when the typical thermopower is zero due to statistical particle-hole symmetry but the mesoscopic fluctuations allow for large thermopower anyway. Van Langen *et al* showed in Ref.[38] that in the localized regime $N \gg \xi$ and for $V_g = 0$, the distribution of the low-temperature thermopower is a Lorentzian,

$$P(S) = \frac{1}{\pi}\frac{\Lambda}{\Lambda^2 + (S-S_0)^2}, \tag{28}$$

with a center $S_0 = 0$ and a width

$$\Lambda = \frac{2\pi t}{\Delta_F} \tag{29}$$

given by $\Delta_F = 1/(N\nu_F)$, the average mean level spacing at E_F. This was derived under certains assumptions

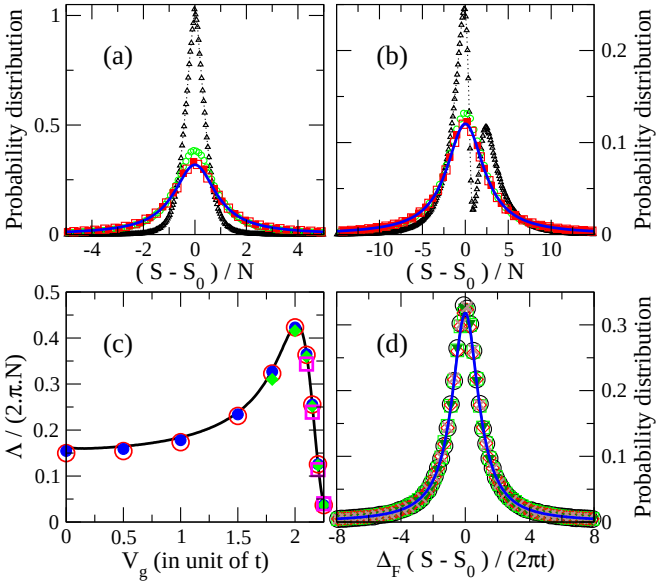

FIG. 5: (Color online) Top panels: probability distributions of the rescaled thermopower $(S - S_0)/N$ at $V_g = 0$ (a) and $V_g = 2t$ (b), with $W = t$, $E_F = 0$ and 1D leads. In each panel, the different symbols correspond to various lengths of the chain ($N \approx \xi$ (△), $N \approx 10\,\xi$ (○), $N \approx 50\,\xi$ (□) and $N \approx 100\,\xi$ (■), respectively $N = 100$, 1000, 5000 and 10000 in (a) and $N = 10$, 100, 500 and 1000 in (b). The distributions obtained for $N \ge 50\,\xi$ collapse on a single curve which is well fitted by a Lorentzian distribution function (thick blue lines). The widths Λ/N of the Lorentzian fits are plotted as a function of V_g in panel (c), for $N = 200$ (□), 1000 (♦), 5000 (○) and 10000 (●), together with the density of states per site at E_F, $t\nu_F$, of the closed chain (red line). The probability distributions of the rescaled thermopower $(\Delta_F/2\pi t)(S - S_0)$, obtained in the large N limit ($N \approx 100\,\xi$) and for various sets of parameters ($W = 0.5t$ and $V_g = 2t$ (◇), $W = t$ and $V_g = 0$ (○), $W = t$ and $V_g = 2t$ (□), $W = 2t$ and $V_g = 0$ (×), and $W = 2t$ and $V_g = 2.3t$ (▼), with $E_F = 0$ in all cases), are shown in panel (d). They all collapse on the blue line which is the Lorentzian function $y = 1/[\pi(1 + x^2)]$.

leading to $S_0 = 0$. As we have shown, $S_0 = 0$ is exact only at the band center ($E_F = 0$), but remains a good approximation in the bulk of the impurity band.

We propose here to investigate how the thermopower distribution $P(S)$ is modified when this is not only the bulk, but the edges (or even the outside) of the impurity band which are probed at the Fermi energy E_F. To fix the ideas, we set the Fermi energy to $E_F = 0$ and the disorder amplitude to $W = t$ (so that the spectrum edges are $V_g + E_c^{\pm} = V_g \pm 2.5t$). First, we check in Fig. 5(a) that at $V_g = 0$ and in the localized regime, the thermopower distribution is indeed a Lorentzian with a width $\Lambda \propto N$. We note that very long chains of length $N \approx 50\xi$ ($\xi \approx 100$ here) are necessary to converge to the Lorentzian (28). Moreover, we have checked that this is also in this limit that the delay time distribution converges towards the universal form predicted in Ref[20].

Then we increase the gate potential up to $V_g = 2t$ to approach the edge E_c^- of the impurity band and find that the thermopower distribution remains a Lorentzian in the localized regime ($N \gtrsim 50\xi$) with a width $\Lambda \propto N$, as shown in Fig. 5(b). It turns out actually that the fit of the thermopower distribution with a lorentzian (in the large N limit) is satisfactory in a broad range of gate potentials $|V_g| \lesssim 2.25t$, as long as the Fermi energy $E_F = 0$ probes the impurity band without approaching too closely its edges $V_g + E_c^{\pm}$. In Fig. 5(c), we show in addition that in this regime, the widths Λ of the Lorentzian fits to the thermopower distributions $P(S)$ obey $\Lambda/(2\pi N t) = \nu_F$, *i.e.* Eq. (29). Therefore (Fig. 5(d)), we can use this parameter to rescale all the distributions obtained in a broad range of parameters, on the same Lorentzian function $y = 1/[\pi(1+x^2)]$. A direct consequence of Eq. (29) is that the mesoscopic fluctuations of the thermopower are maximal for $|E_F - V_g| \approx 2t$.

When the gate voltage $|V_g|$ is increased further, the number of states available at E_F in the nanowire decreases exponentially and eventually vanishes: one approaches eventually a regime where the nanowire becomes a long tunnel barrier and where the thermopower fluctuations are expected to be smaller and smaller. In this limit, we find that the thermopower distribution is no more a Lorentzian but becomes a Gaussian,

$$P(S) = \frac{1}{\sqrt{2\pi}\lambda} \exp\left[-\frac{(S-S_0)^2}{2\lambda^2}\right], \qquad (30)$$

provided the chain is long enough. This result is illustrated in Figs. 6(a) and 6(b) for two values of V_g. The Gaussian thermopower distribution is centered around a typical value S_0 given by Eq. (27) and its width λ is found with great precision to increase linearly with $\sqrt{N}$ and W. To be more precise, we find that the dependency of λ on the various parameters is mainly captured by the following formula

$$\lambda \approx 0.6 \frac{Wt\sqrt{N}}{(E_F - V_g)^2 - (2t + W/4)^2}, \qquad (31)$$

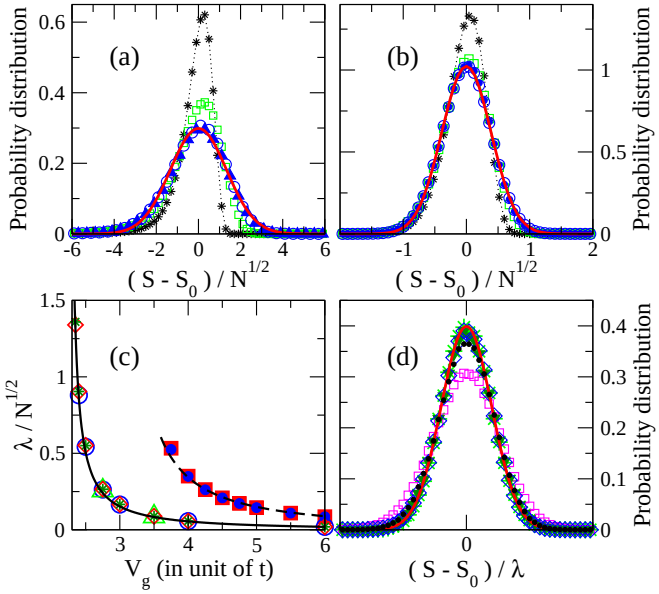

FIG. 6: (Color online) Top panels: probability distributions of the rescaled thermopower $(S - S_0)/\sqrt{N}$ at $V_g = 2.35t$ (a) and $V_g = 2.6t$ (b), with $W = t$, $E_F = 0$ and 1D leads. In each panel, the distributions are plotted for various lengths of the chain ($N = 10$ (∗), 50 (□), 200 (●), 500 (○) and 1000 (▲)) and collapse at large N on one single curve, well fitted by a Gaussian distribution (red line). The widths $\lambda/\sqrt{N}$ of the Gaussian fits are plotted as a function of V_g in panel (c), for various lengths ($N = 50$ (triangle), 200 (circle), 400 (square), 800 (diamond) and 1600 (star)) and two disorder amplitudes ($W = t$ (empty symbols) and $W = 4t$ (full symbols)). The solid and dashed lines are the fits given by Eq. (31), respectively for $W = t$ and $W = 4t$. Panel (d): collapse of the thermopower distributions, obtained with $N = 500$ and various parameters ($W = 0.5t$ and $V_g = 2.25t$ (□), $W = 0.5t$ and $V_g = 5t$ (▼), $W = t$ and $V_g = 2.5t$ (●), $W = t$ and $V_g = 5t$ (∗), and $W = 4t$ and $V_g = 4t$ (◊)), after a rescaling by λ as given in Eq. (31). The red line is the Gaussian distribution $y = (1/\sqrt{2\pi})\exp(-x^2/2)$.

at least for $0.5t \lesssim W \lesssim 4t$, $2.35t \lesssim |E_F - V_g| \lesssim 6t$ and $N \gtrsim 100$ (see Fig. 6(c)). We stress out that Eq. (31) is merely a compact way of describing our numerical data. In particular, the apparent divergence of λ when $|E_F - V_g| \to 2t + W/4$ is meaningless and in fact, it occurs outside the range of validity of the fit. To double-check the validity of Eq. (31), we have rescaled with the parameter λ given by Eq. (31), a set of thermopower distributions obtained in the disordered tunnel barrier regime, for various W and V_g. All the resulting curves (plotted in Fig. 6(d)) are superimposed on the unit gaussian distribution, except the one for the smallest disorder value $W = 0.5t$ for which the fit (31) to λ is satisfactory but not perfect.

To identify precisely the position of the crossover between the Lorentzian regime and the Gaussian regime,

we introduce now the parameter η,

$$\eta = \frac{\int dS|P(S) - P_G(S)|}{\int dS|P_L(S) - P_G(S)|}, \tag{32}$$

which measures, for a given thermopower distribution $P(S)$ obtained numerically, how closed it is from its best Gaussian fit $P_G(S)$ and from its best Lorentzian fit $P_L(S)$[46]. If $P(S)$ is a Lorentzian, $\eta = 1$ while $\eta = 0$ if it is a Gaussian. Considering first the case where $E_F = 0$ and $W = t$, we show in the left panel of Fig. 7 that η converges at large N for any V_g (inset). The asymptotic values of η (given with a precision of the order of 0.05 in the main panel) undergo a transition from $\eta \approx 1$ to $\eta \approx 0$ when V_g is increased from 0 to $4t$. This reflects the crossover from the Lorentzian to the Gaussian thermopower distribution already observed in the top panels of Figs. 5 and 6. We see in addition that the crossover is very sharp around the value $V_g \approx 2.3t$, indicating a crossover which remains inside the impurity band of the nanowire, since the band is not shifted enough when $V_g \approx 2.3t$ to make the Fermi energy coincides with the band edge $V_g + E_c^- = V_g - 2.5t$. We have obtained the same results for other values of the disorder amplitude. After checking the convergence of η at large N, we observe the same behavior of the asymptotic values of η as a function of V_g, for any W. Only the position of the crossover is disorder-dependent. Those results are summarized in the right panel of Fig. 7 where one clearly sees the crossover (in white) between the Lorentzian regime (in blue) and the Gaussian regime (in red). It occurs around $V_g \approx 1.92t + 0.34W$, not exactly when $E_F = V_g + E_c^-$, but in a region where the number of states available at E_F in the nanowire becomes extremely small. To be precise, we point out that the values of η in the 2D colorplot are given with a precision of the order of 0.1. Hence, one cannot exclude that the white region corresponding to the crossover actually reduces into a single line $V_g^c(W)$. One could also conjecture the existence of a third kind of thermopower distribution (neither Lorentzian, nor Gaussian) associated to this critical value V_g^c. Our present numerical results do not allow to favor one scenario (sharp crossover) over the other (existence of a critical edge distribution).

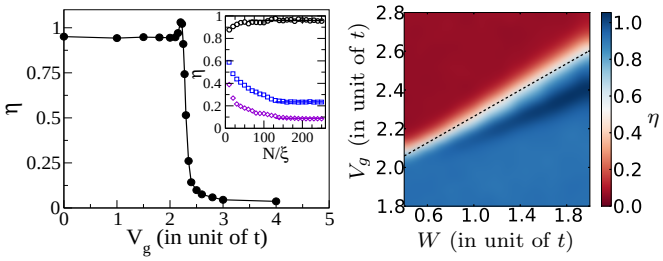

FIG. 7: (Color online) Left panel: in the inset, η parameter as a function of N/ξ for various gate voltages ($V_g = 1.9\,t$ (○), $2.35\,t$ (□) and $2.5\,t$ (◇)), at $E_F = 0$ and $W/t = 1$. The horizontal lines show the convergence of η at large N. The asymptotic values are plotted in the main panel as a function of V_g. Right panel: η parameter in the limit of large N as a function of V_g and W, at $E_F = 0$. Upon shifting the spectrum of the nanowire with V_g, the thermopower distribution moves from a Lorentzian distribution for $V_g \lesssim V_g^c$ ($\eta \approx 1$, blue) to a Gaussian distribution for $V_g \gtrsim V_g^c$ ($\eta \approx 0$, red), where $V_g^c = 1.92t + 0.34W$ (dashed line).

VI. FIGURE OF MERIT

Within linear response, the efficiency of steady state heat to work conversion reads

$$\eta = \frac{\dot{W}}{\dot{Q}} = \frac{I_e \Delta\mu}{I_Q}, \tag{33}$$

where $I_Q > 0$ is the heat injected, while the numerator is the output power. One could maximize this expression with respect to $\Delta\mu$ to calculate the *maximum efficiency*[39] η_{max}, or rather maximize the output power $P = I_e \Delta\mu$ and look then at the *efficiency at maximum power*[40] $\eta(P_{max})$. Both these two efficiencies turn out to depend only on a dimensionless quantity, known as the thermoelectric *figure of merit*[47] $ZT = (G\mathcal{S}^2/\kappa_e)\,T$, as

$$\eta_{max} = \eta_C \frac{\sqrt{ZT+1}-1}{\sqrt{ZT+1}+1}$$
$$\eta(P_{max}) = \frac{\eta_C}{2}\frac{ZT}{ZT+2} \tag{34}$$

η_C being the Carnot efficiency. In particular, they are both monotonous growing functions of ZT, being equal to 0 for $ZT = 0$, while $\eta_{max} \to \eta_C$ and $\eta(P_{max}) \to \eta_C/2$ for $ZT \to \infty$. Note that, for small ZT, $\eta_{max} \approx \eta(P_{max}) \approx (\eta_C/4)ZT$, the difference between the two efficiencies becoming relevant only for $ZT > 1$. In any case, by virtue of the above equations, it is clear that maximizing the figure of merit is the necessary condition in order to achieve the largest efficiencies. In the low-temperature regime we investigate, the Wiedemann-Franz law is valid and thus the figure of merit can be written as

$$ZT = \mathcal{S}^2 \frac{GT}{\kappa_e} = \frac{\mathcal{S}^2}{\mathcal{L}_0}, \tag{35}$$

meaning that ZT is simply the square of the thermopower, up to a constant (the Lorenz number). In Fig. 8 we show the typical behavior of the figure of merit as a function of the gate voltage V_g and the size of the system N. Note that it is related to the dimensionless thermopower S studied in this work by $ZT = S^2(\pi^2/3)(k_BT/t)^2$. The typical value ZT_0 has been defined by exponentiating the median of the distribution of the logarithm of ZT. We have chosen to do so because the distribution $P(ZT)$ exhibits a singularity[48] for ZT, while $P(\ln(ZT))$ turns out to be a symmetric,

smooth function. Not surprisingly, Fig. 8 shows that the enhancement of the typical thermopower around the edges reflects in a larger figure of merit. Moreover, being $S_0 \propto \mathrm{d}[\ln \mathcal{T}]_0/\mathrm{d}E \propto N$, we expect $ZT_0 \propto N^2$, i.e. the longer the wire is, the better should be in terms of the figure of merit. Despite this, our theory which is only valid in a low-temperature limit cannot predict high performances: even supposing to be at the highest temperature ($\sim T_s$, see Sec. VII) where Sommerfeld expansions can be made for describing the thermopower with Eq.(10), the region of largest ZT_0 in Fig. 8 corresponds to values of order $ZT_0 \lesssim 0.024$ at $k_BT/t = 5 \times 10^{-5}$. We emphasize that this low figure of merit characterizes the very low temperatures where Sommerfeld expansion holds, but by no means this sets a physical limit to the efficiency. On the other hand, if we were to look to the delivered (electric) output power, we would find that a large size would make it vanish, as the electrical conductance in this regime would be exponentially small. Indeed, looking at the power factor $\mathcal{Q} = \mathcal{S}^2 G$, which is a measure of the maximum output power[40], we realize that the enhancement of $\mathcal{S}$ at the edge of the impurity band would not be enough to face the exponentially small values of G. Obviously, the optimization of the power factor $\mathcal{Q}$ for a single nanowire requires to take shorter sizes ($N \approx \xi$), while the optimization of the figure of merit ZT requires to take long sizes ($N \gg \xi$). Moreover, because of the strong variation of the localization length as the energy varies inside the impurity band, the optimization of the power factor for a given size N requires to not be too close from the edges of the impurity band, contrary to the optimization of the efficiency. This illustrates the fact that a compromise has always to be found between efficiency and output power when thinking of practical thermoelectric applications. A possibility would be to optimize the efficiency at a given output power. More interestingly, one could also study an ensemble of nanowires in parallel instead of a single one. Since the conductances in parallel add while the thermopower does not scale with the number of wires, the compromise will favor the limit of long nanowires with applied gate voltages such that electron transport occurs near the edges of impurity bands.

VII. TEMPERATURE RANGE OF VALIDITY OF THE SOMMERFELD EXPANSION

All the results discussed in this paper have been obtained in the low temperature limit, after expanding the thermoelectric coefficients to the lowest order in k_BT/E_F. To evaluate the temperature range of validity of this study, we have calculated the Lorenz number $\mathcal{L} = \kappa_e/GT$ beyond the Sommerfeld expansion, and looked at its deviations from the WF law $\mathcal{L} = \mathcal{L}_0$ (see Eq. (11)): We have computed numerically the integrals (4) enterings Eqs. (5) and (6), deduced $\mathcal{L}(T)$ for increasing values of temperature, and then recorded the temperature T_s above which $\mathcal{L}(T)$ differs from $\mathcal{L}_0$ by a

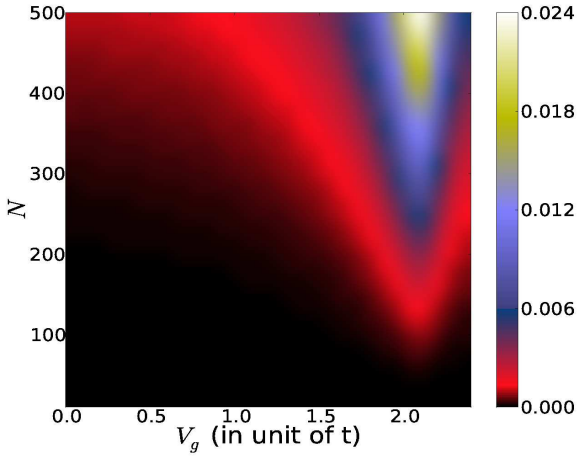

FIG. 8: (Color online) Typical value of the figure of merit $ZT = \mathcal{S}^2/\mathcal{L}_0 = \pi^2/3(k_BT/t)^2 S^2$ as a function of V_g and N, at $E_F = 0$, $W = t$, and for a very low temperature $k_BT/t = 5 \times 10^{-5}$ (which is nevertheless the highest temperature below which the Sommerfeld expansion is valid, for all $N \leq 500$ and $V_g \leq 2.5t$, within a tolerance of $\sim 2\%$, see Sec. VII). Being proportional to S^2 in the regime of validity of the Wiedemann-Franz law, the largest typical figures of merit are obtained around the edge of the impurity band and for long wires.

percentage ϵ, $\mathcal{L}(T_s) = \mathcal{L}_0(1 \pm \epsilon)$. We did it sample by sample and deduced the temperature T_s averaged over disorder configurations. Our results are summarized in Fig. 9.

In panel (a), we analyze how sensitive T_s is to the precision ϵ on the Lorenz number $\mathcal{L}$. We find that T_s increases linearly with $\sqrt{\epsilon}$, $T_s(\epsilon) = T_s^* \sqrt{\epsilon}$, at least for $\epsilon \leq 2\%$. This is not surprising since the Sommerfeld expansion leads to $\mathcal{L} - \mathcal{L}_0 \propto (k_BT)^2$, when one does not stop the expansion to the leading order in temperature ($\mathcal{L} = \mathcal{L}_0$) but to the next order.

The main result of this section is shown in Fig. 9(b) where we have plotted the temperature T_s as a function of the gate voltage V_g, for chains of different lengths, at fixed $E_F = 0$ and $W = t$. As long as the Fermi energy probes the inside of the spectrum without approaching too much its edges ($|V_g| \leq 2t$), T_s is found to decrease as V_g is increased. More precisely, we find in the large N limit ($N \gtrsim 10\xi$) that $N k_B T_s \propto \nu_F^{-1}$ with a proportionality factor depending on ϵ (solid line in Fig. 9(b)). The temperature T_s is hence given by (a fraction) of the mean level spacing at E_F in this region of the spectrum ($k_BT_s \propto \Delta_F$). When V_g is increased further, T_s reaches a minimum around $|V_g| \approx 2.1t$ and then increases sharply. Outside the spectrum, this increase of T_s with V_g is well understood as follows: Since in the tunnel barrier regime, the transmission behaves (upon neglecting the disorder effect) as $\mathcal{T} \propto \exp(-N\kappa)$, with $\kappa = \cosh^{-1}[|E - V_g|/(2t)]$, the temperature scale below which the Sommerfeld expansion of integrals (4) holds is given by $k_BT_s \propto [N \frac{\mathrm{d}\kappa}{\mathrm{d}E}\big|_{E_F}]^{-1}$, which yields $N k_B T_s \propto$

$t\sqrt{[(E_F - V_g)/(2t)]^2 - 1}$. Our numerical results are in perfect agreement with this prediction (dashed line in Fig. 9(b)).

In Fig. 9(c), we investigate the behavior of T_s when the spectrum of the nanowire is either scanned by varying V_g at $E_F = 0$ or by varying E_F at $V_g = 0$. We find that T_s only depends on the part of the impurity band which is probed at E_F (*i.e.* the curves $T_s(V_g)$ and $T_s(E_F)$ are superimposed), except when E_F approaches closely one edge of the conduction band of the leads. In that case, T_s turns out to drop fast to zero as it can be seen in Fig. 9(c) for the case of 1D leads ($T_s \to 0$ when $E_F \to 2t$). This means that the divergence of the *dimensionless* thermopower S observed in Fig. 4(a) is only valid in an infinitely small range of temperature above 0 K. It would be worth figuring out wether or not a singular behavior of the thermopower at the band edges of the conduction band persists at larger temperature.

Let us give finally an order of magnitude in Kelvin of the temperature scale T_s. In Fig. 9(b), the lowest T_s reached around $V_g \approx 2.1t$ is about $Nk_BT_s^{min}/t \sim 0.001$ for $\epsilon = 0.004\%$. Asking for a precision of $\epsilon = 1\%$ on $\mathcal{L}$, we get $Nk_BT_s^{min}/t \sim 0.016$. For a bismuth nanowire of length 1 μm with effective mass $m^* = 0.2m_e$ (m_e electron mass) and lattice constant $a = 4.7$ Å, the hopping term evaluates at $t = \hbar^2/(2m^*a^2) \sim 0.84$ eV and hence, $T_s^{min} \sim 72$ mK. The same calculation for a silicon nanowire of length 1 μm with $m^* = 0.2m_e$ and a =5.4 Å yields $T_s^{min} \sim 64$ mK. Those temperatures being commonly accessible in the laboratories, the results discussed in this paper should be amenable to experimental checks.

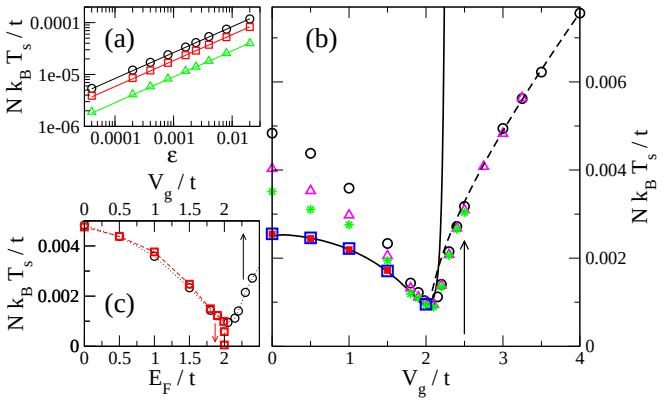

FIG. 9: (Color online) Temperature scale T_s above which the WF law breaks down. (a) Nk_BT_s/t as a function of the desired precision ϵ on $\mathcal{L}$. The critical temperatures were extracted for different values of V_g ($V_g = t$ (○), $1.5t$ (□), $2.02t$ (△)), with $E_F = 0$, $W/t = 1$, $N = 500$ and 1D leads. The solid lines are fits $T_s = T_s^*\sqrt{\epsilon}$. (b) Nk_BT_s/t (extracted for $\epsilon = 4 \times 10^{-5}$) as a function of V_g/t, for chains of different length ($N = 150$ (○), 300 (△), 500 (∗), 1500 (□) and 3000 (■)), with $E_F = 0$, $W/t = 1$ and 1D leads. The solid line is $4.04 \times 10^{-4}/(\nu_F t)$, the dashed line is $4.37 \times 10^{-3}\sqrt{(V_g/2t)^2 - 1}$ and the arrow indicates the position of the edge of the impurity band. (c) Nk_BT_s/t (extracted for $\epsilon = 4 \times 10^{-5}$) as a function of E_F/t at $V_g = 0$ (□) and as a function V_g/t at $E_F = 0$ (○), with $N = 150$, $W/t = 1$ and 1D leads. Dashed lines are guides to the eye.

VIII. CONCLUSION

We have systematically investigated the low-temperature behavior of the thermopower of a single nanowire, gradually depleted with a gate voltage in the field effect transistor device configuration. Disorder-induced quantum effects, unavoidable in the low-temperature coherent regime, were properly taken into account. We have provided a full analytical description of the behavior of the typical thermopower as a function of the gate voltage and have confirmed our predictions by numerical simulations. Our results show that the typical thermopower is maximized when the Fermi energy lies in a small region inside the impurity band of the nanowire, close to its edges. Moreover, since thermoelectric conversion strongly varies from one sample to another in the coherent regime, we have carefully investigated the mesoscopic fluctuations of the thermopower around its typical value. We have shown that the thermopower is Lorentzian-distributed inside the impurity band of the nanowire and that its fluctuations follow the behavior of the density of states at the Fermi energy when the gate voltage is varied. In the vicinity of the edges of the impurity band and outside the band, the thermopower was found Gaussian-distributed with tiny fluctuations.

Electron-electron interactions were not included in our study. A comprehensive description of the thermopower of a 1D disordered nanowire should definitely consider them. Nevertheless, we expect that the drastic effects of electronic correlations in 1D leading to the formation of a Luttinger liquid are somehow lightened by the presence of disorder. Second, the gate modulation of the thermopower we predict here is mainly due to a peculiar behavior of the localization length close to the edges of the impurity band. And experimentally, coherent electronic transport in gated quasi-1D nanowires turned out to be well captured with one-electron interference models[41]. Of course, one could think of including electronic interactions numerically with appropriate numerical 1D methods but regarding the issue of thermoelectric conversion in nanowires, we believe the priority rather lies in a proper treatment of the phonon activated inelastic regime.

Finally, let us discuss the potential of our results for future nanowire-based thermoelectric applications. One cannot reach high values of ZT and extract much electric power from a nanowire, when one restricts oneself to the very low temperature regime. If one wants to use a nanowire as a thermoelectric generator, one should consider higher temperatures, where electronic transport can be thermally activated[42]. It will be the purpose of our next paper[7]. Actually, when thinking of

practical applications, the results of the present paper are rather promising regarding Peltier refrigeration. Indeed, our conclusions drawn here for the thermopower at low temperature also hold for the Peltier coefficient, the two being related by the Kelvin-Onsager relation $\Pi = \mathcal{S}T$. One could imagine to build up Peltier modules with doped nanowires for cooling down a device at sub-Kelvin temperature in a coherent way. Besides, whether it be for energy harvesting or Peltier cooling, it would be worth considering more complicated setups using the nanowire as a building block (e.g. sets of parallel nanowires in the field effect transistor device configuration) in order to reach larger values of output electric/cooling power.

Acknowledgments

This work has been supported by CEA through the DSM-Energy Program (project E112-7-Meso-Therm-DSM).

Appendix A: Self-energy of the 2D leads

We give here the expression of the retarded self-energy of a 2D lead (made of a semi-infinite square lattice with hopping term t) connected at one site (with coupling t) to a nanowire of N sites length. It is a $N \times N$ matrix Σ with only one non-zero component denoted σ. To calculate σ, we calculate first the retarded Green's function of an infinite square lattice[32] and then deduce with the method of mirror images the retarded Green's function of the semi-infinite 2D lead[43], that we evaluate at the site in the lead coupled to the nanowire to get σ. Analytic continuations of special functions are also required, they can be found for example in Ref.[44]. Introducing the notation $z = E/(4t)$, we find for $\sigma = \mathrm{Re}(\sigma) + i\,\mathrm{Im}(\sigma)$

$$\mathrm{Re}(\sigma) = tz \pm \frac{2t}{\pi}\left[\mathcal{E}(z^2) - (1-z^2)\mathcal{K}(z^2)\right] \tag{A1}$$

$$\mathrm{Im}(\sigma) = \frac{2t}{\pi}\left[-\mathcal{E}(1-z^2) + z^2\mathcal{K}(1-z^2)\right] \tag{A2}$$

with a + sign in Eq. (A1) when $-4t \leq E \leq 0$ and a − sign when $0 \leq E \leq 4t$. If the energy E is outside the conduction band of the lead ($|E| > 4t$), we get

$$\sigma = tz\left[1 - \frac{2}{\pi}\mathcal{E}\left(\frac{1}{z^2}\right)\right]. \tag{A3}$$

In the three above equations, $\mathcal{K}$ and $\mathcal{E}$ stand for the complete elliptic integrals of the first and second kind respectively. They are defined as

$$\mathcal{K}(z) = \int_0^{\pi/2} d\phi\,[1 - z\sin^2\phi]^{-1/2} \tag{A4}$$

$$\mathcal{E}(z) = \int_0^{\pi/2} d\phi\,[1 - z\sin^2\phi]^{1/2}. \tag{A5}$$

Appendix B: Thermopower of a clean tunnel barrier

In this appendix, we derive Eq. (27). We consider a clean nanowire with on-site potentials V_g, connected via its extreme sites 1 and N to two identical semi-infinite leads. In order to investigate the tunnel barrier regime, we assume that the energy E of the incoming electrons lies outside the spectrum $[-2t, 2t]$ of the nanowire. Let us say that $E \geq V_g + 2t$ to fix the ideas. In the basis $\{1, N, 2, ..., N-2\}$, the retarded Green's function $G = [E - \mathcal{H} - \Sigma_L - \Sigma_R]^{-1}$ of the system reads

$$G = \begin{pmatrix} A & B \\ \tilde{B} & C \end{pmatrix}^{-1} \tag{B1}$$

where *(i)* $A = (E - V_g - \sigma)\mathbf{1_2}$ ($\mathbf{1_2}$ being the 2×2 identity matrix and σ the non-vanishing element of Σ_L and Σ_R), *(ii)* B [$\tilde{B}$] is a $2 \times (N-2)$ [$(N-2)\times 2$] matrix with all zero components except two equal to t coupling the sites 1 and N to their neighbors 2 and $N-1$, and *(iii)* C is a $(N-2)\times(N-2)$ symmetric tridiagonal matrix with all diagonal elements equal to $E - V_g$ and all elements on the first diagonals below and above the main one equal to t. Using the Fisher-Lee formula (14), we write the transmission function $\mathcal{T}(E)$ as

$$\mathcal{T}(E) = \mathrm{Tr}\left[\begin{pmatrix}\gamma & 0\\ 0 & 0\end{pmatrix} G_A \begin{pmatrix}0 & 0\\ 0 & \gamma\end{pmatrix} G_A^\dagger\right] \tag{B2}$$

$$= \gamma^2 |G_A^{(1N)}|^2 \tag{B3}$$

where G_A is the 2×2 submatrix in the top left-hand corner of G, $G_A^{(1N)}$ its top right element and $\gamma = -2\mathrm{Im}(\sigma)$. To calculate G_A, we first notice that

$$G_A = (A - BC^{-1}\tilde{B})^{-1} = (A - t^2 C_\square^{-1})^{-1} \tag{B4}$$

where $C_\square^{-1}$ is a 2×2 submatrix of C^{-1} made up of the four elements located at its four corners. Second, we make use of Ref.[45] for computing the inverse of the symmetric tridiagonal matrix C. We get

$$C_\square^{-1} = \begin{pmatrix}\alpha & \beta\\ \beta & \alpha\end{pmatrix} \tag{B5}$$

with

$$\alpha = -\frac{\cosh(\kappa)\cosh((N-2)\kappa)}{t\sinh(\kappa)\sinh((N-1)\kappa)} \tag{B6}$$

$$\beta = -\frac{\cosh(2\kappa) + (-1)^{N-1}}{2t\sinh(\kappa)\sinh((N-1)\kappa)} \tag{B7}$$

and $\kappa = \cosh^{-1}[(E - V_g)/(2t)]$. Plugging Eqs. (B4-B7) into Eq. (B3), we deduce the exact transmission function $\mathcal{T}(E)$, and hence the thermopower S defined by Eq. (15). An expansion at large N yields $\mathcal{T} \propto \exp(-2N\kappa)$ (as expected for a tunnel barrier) and the expression (27) for the thermopower. The same demonstration can be made for the energy range $E \leq V_g - 2t$.

[1] L. D. Hicks and M. S. Dresselhaus, Phys. Rev. B **47**, 16631 (1993).
[2] A. I. Hochbaum, R. Chen, R. D. Delgado, W. Liang, E. C. Garnett, M. Najarian, A. Majumdar, and P. Yang, Nature **451**, 163 (2008).
[3] A. I. Boukai, Y. Bunimovich, J. Tahir-Kheli, J.-K. Yu, W. A. Goddard, and J. R. Heath, Nature **451**, 168 (2008).
[4] P. Martin, Z. Aksamija, E. Pop, and U. Ravaioli, Phys. Rev. Lett. **102**, 125503 (2009).
[5] G. D. Mahan and J. O. Sofo, Proc. Natl. Acad. Sci. USA **93**, 7436 (1996).
[6] Y. Tian, M. R. Sakr, J. M. Kinder, D. Liang, M. J. MacDonald, R. L. J. Qiu, H.-J. Gao, and X. P. A. Gao, Nano Lett. **12**, 6492 (2012).
[7] R. Bosisio, G. Fleury, and J.-L. Pichard, Paper in preparation (2013).
[8] Y.-M. Lin, X. Sun, and M. S. Dresselhaus, Phys. Rev. B **62**, 4610 (2000).
[9] N. Mingo, Appl. Phys. Lett. **84**, 2652 (2004).
[10] N. Neophytou and H. Kosina, Phys. Rev. B **83**, 245305 (2011).
[11] G. Liang, W. Huang, C. S. Koong, J.-S. Wang, and J. Lan, J. Appl. Phys. **107**, 014317 (2010).
[12] W. Liang, A. I. Hochbaum, M. Fardy, O. Rabin, M. Zhang, and P. Yang, Nano Lett. **9**, 1689 (2009).
[13] Y. Zuev, J. S. Lee, C. Galloy, H. Park, and P. Kim, Nano Lett. **10**, 3037 (2012).
[14] J. Moon, J.-H. Kim, Z. C. Y. Chen, J. Xiang, and R. Chen, Nano Lett. **13**, 1196 (2013).
[15] P. M. Wu, J. Gooth, X. Zianni, S. Fahlvik Svensson, J. G. Gluschke, K. A. Dick, C. Thelander, K. Nielsch, and H. Linke, Nano Lett. **13**, 4080 (2013).
[16] Y. M. Brovman, J. P. Small, Y. Hu, Y. Fang, C. M. Lieber, and P. Kim, arXiv:1307.0249 (2013).
[17] N. F. Mott and E. A. Davis, *Electronic Processes in Non Crystalline Materials* (Clarendon, Oxford, 1979), 2nd ed.
[18] P. W. Anderson, D. J. Thouless, E. Abrahams, and D. S. Fisher, Phys. Rev. B **22**, 5319 (1980).
[19] J.-L. Pichard, J. Phys. C: Solid State Phys. **19**, 1519 (1986).
[20] C. Texier and A. Comtet, Phys. Rev. Lett. **82**, 4220 (1999).
[21] S. Datta, *Electronic Transport in Mesoscopic Systems* (Cambridge University Press, 1995).
[22] P. N. Butcher, J. Phys.: Condens. Matter **2**, 4869 (1990).
[23] L. Onsager, Phys. Rev. **37**, 405 (1931).
[24] H. B. G. Casimir, Rev. Mod. Phys. **17**, 343 (1945).
[25] N. W. Ashcroft and N. D. Mermin, *Solid state physics* (Saunders College Publishing, 1976).
[26] V. Balachandran, R. Bosisio, and G. Benenti, Phys. Rev. B **86**, 035433 (2012).
[27] M. G. Vavilov and A. D. Stone, Phys Rev. B **72**, 205107 (2005).
[28] G. V. Chester and A. Thellung, Proc. Phys. Soc. **77**, 1005 (1961).
[29] C. L. Kane and M. P. A. Fisher, Phys. Rev. Lett. **76**, 3192 (1996).
[30] N. Wakeham, A. F. Bangura, X. Xu, J.-F. Mercure, M. Greenblatt, and N. E. Hussey, Nat. Commun. **2**, 396 (2011).
[31] A. Lassl, P. Schlagheck, and K. Richter, Phys. Rev. B **75**, 045346 (2007).
[32] E. N. Economou, *Green's functions in quantum physics* (Springer, 2006), 3rd ed.
[33] B. Derrida and E. Gardner, J. Physique **45**, 1283 (1984).
[34] J.-L. Pichard, in *Quantum Coherence in Mesoscopic Systems,* NATO ASI Series, Series B: Phys. vol. 254, ed. B. Kramer (Plenum Press, 1990).
[35] A. D. Stone, P. A. Mello, K. A. Muttalib, and J.-L. Pichard, in *Mesoscopic Phenomena in Solids,* vol. 30, ed. B. L. Altschuler, P. A. Lee and R. A. Webb (North-Holland, 1991).
[36] B. Kramer and A. MacKinnon, Rep. Prog. Phys. **56**, 1469 (1993).
[37] M. Kappus and E. Wegner, Z. Phys. B **45**, 15 (1981).
[38] S. A. van Langen, P. G. Silvestrov, and C. W. J. Beenakker, Supperlattices Microstruct. **23**, 691 (1998).
[39] H. Callen, *Thermodynamics and an Introduction to Thermostatics* (John Wiley and Sons, New York, 1985).
[40] C. Van den Broeck, Phys Rev. Lett. **95**, 190602 (2005).
[41] W. Poirier, D. Mailly, and M. Sanquer, Phys. Rev. B **59**, 10856 (1999).
[42] J.-H. Jiang, O. Entin-Wohlman, and Y. Imry, Phys. Rev. B **85**, 075412 (2012).
[43] M. I. Molina, Phys. Rev. B **74**, 045412 (2006).
[44] T. Morita, J. Math. Phys. **12**, 1744 (1971).
[45] G. Y. Hu and R. F. O'Connell, J. Phys. A: Math. Gen. **29**, 1511 (1996).
[46] One could be tempted to compare an arbitrary thermopower distribution $P(S)$ to the Lorentzian and Gaussian distributions given in Eqs. (28 - 29) and (30 - 31) respectively. However, to define η for any set of parameters, one should extend to the outside of the spectrum the formula (29) for the width Λ of the Lorentzian, and to the inside of the spectrum the formula (31) for the width λ of the Gaussian. We avoid this problem by taking instead the best Lorentzian and Gaussian fits to $P(S)$ in the definition of η. It allows us to distinguish whether $P(S)$ is a Lorentzian or a Gaussian (or none of both) but of course, the precise form of $P(S)$ is not probed by η as defined.
[47] In principle, the thermal conductance appearing in the definition of ZT should be the sum of an electronic and a phononic contribution, $\kappa = \kappa_e + \kappa_{ph}$. Since we are interested in a low-temperatures coherent regime, we assume κ_{ph} to be negligible, compared to κ_e, and hence $\kappa \approx \kappa_e$.
[48] This can be also seen by calculating $P(ZT)$ analytically from Eq. (28)